

Solid–Solid and Solid–Fluid Equilibria of the Most Popular Models of Methanol Obtained by Computer Simulation

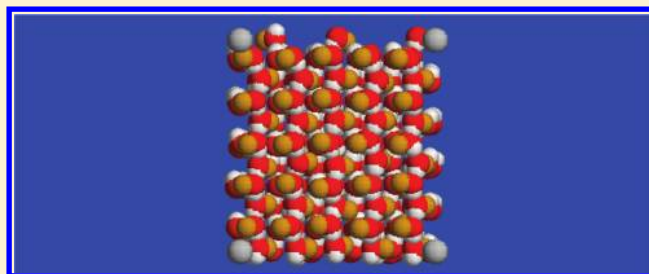
D. Gonzalez-Salgado,^{*,†} A. Dopazo-Paz,[†] P. Gomez-Alvarez,[†] J. M. Miguez,[†] and C. Vega[‡]

[†]Universidad de Vigo, Departamento de Física Aplicada, As Lagoas s/n, 32004, Ourense, Spain

[‡]Universidad Complutense de Madrid, Facultad de Ciencias Químicas, Departamento de Química Física, 28040 Madrid, Spain

S Supporting Information

ABSTRACT: The ability of the most popular models of methanol (H1, OPLS, L2, and L1) for the prediction of the solid–solid and the solid–fluid equilibria was analyzed in detail in this work by using molecular simulation. The three solid phases (α , β , and γ) detected experimentally as being thermodynamically stable, as well as the fluid phase, were considered for the calculations. It turns out that all the models provide similar results. The α , γ , and fluid phases were found to be thermodynamically stable for a certain range of temperatures and pressures, whereas the β phase was always metastable. The coexistence curves (α –fluid, α – γ , γ –fluid) corresponding to all the models took the same shape except for some slight differences about their locations. From a qualitative point of view, it can be considered that the four models give a reasonable prediction of the phase diagram of methanol. However, there are important quantitative discrepancies. The melting points fell in the interval 214–223 K, whereas the γ phase was predicted to be stable at pressures above 12×10^4 bar. These results are quite different in relation to the experiments since the melting point of methanol is 175.6 K and the γ phase is stable at 3.5×10^4 bar at room temperature. In addition, the values of the melting enthalpy obtained by the different models are very similar but about 50% higher than the experimental value. Therefore, it is clear that there is room for improvement. Reducing the stability of the α phase with respect to the other phases seems to be a necessary condition to construct an improved potential.



INTRODUCTION

Methanol is one of the most studied substances due to both its variety of industrial applications and its importance in basic research. Apart from its well-known suitability as a solvent, it is frequently used, among other applications, as a truly hydrostatic medium up to 10×10^4 bar,^{1,2} as a cosolvent to stabilize nanoparticles at interfaces,³ in natural gas pipelines to avoid the formation of methane hydrates,⁴ as fuel,⁵ and in solar thermal systems.⁶ In the field of fundamental investigation, methanol is commonly used to study the physics of associated systems since it is, maybe after water and ammonia, the simplest molecule forming hydrogen bonds. Moreover, it is considered to be a prototype molecule to elucidate the theoretical grounds of the hydrophobic interaction in aqueous solutions due to its amphiphilic character with a polar group and an apolar head. It is believed that a full understanding of aqueous solutions of methanol may provide insights into the behavior of certain biological systems.⁷ As a consequence, the thermodynamic behavior of methanol has been extensively studied for the fluid phase^{8–11} and up to a certain point for the solid phases.^{12–19} Three different solid structures, namely, α , β , and γ , have been found to date. The β phase coexists with the fluid in the pressure range (0 – 1×10^4) bar. At lower temperatures, the α phase is the thermodynamically stable one; the coexistence line between

α and β phases expands along the same pressure interval and is separated by about 15 K from the fluid– β line. The α and β phases are both orthorhombic of space groups $P2_12_12_1$ and $Cmcm$, respectively. The γ phase is a high density triclinic solid with space group $P\bar{1}$. It was found to be the stable solid at $T = 298$ K and $p = 3.5 \times 10^4$ bar.

A large body of work has been devoted to the construction of an intermolecular potential model for methanol to be used in molecular simulation. The proposed models present different degrees of complexity, going from the simple pairwise additive potentials based on the rigid molecule approximation^{20–30} to more complex descriptions including flexibility,^{24,26,31–35} polarizability,^{36,37} or both.^{38–41} The most widely used models are the rigid ones since they are able to qualitatively describe the thermodynamic and structural features of this substance in spite of their simplicity. In this group, the Optimised Potential for Liquid Simulations (OPLS) model proposed by Jorgensen,²⁰ the H1 model of Haughney et al.,^{21,22} the L1 model of Van Leeuwen and Smit,²³ and the L2 model of Hasse and co-workers^{27,28} must be mentioned as the most popular ones. All of them are three-site

Received: October 21, 2010

Revised: February 2, 2011

Published: March 10, 2011

models, with one site representing the methyl group, another site on the oxygen atom, and a third site on the hydrogen of the hydroxyl group. These sites are located spatially according to the geometry of methanol obtained from microwave studies.⁴² Differences between them reside in the values of the Lennard-Jones parameters and the charges on the sites. The parameters corresponding to OPLS and H1 models were obtained by fitting to thermodynamic properties at room conditions and to some results determined by using quantum mechanical calculations. The L1 and L2 models belong to a new class of models which are constructed to reproduce thermodynamic properties at several temperatures, in this case, the vapor–liquid equilibrium. All these models have been mainly used to simulate methanol in the fluid phase or even in the glassy state. However, little attention has been paid to the study of the solid phases. To our knowledge, the solid–solid and solid–fluid equilibrium (SSE and SFE) has only been calculated recently by the authors⁴³ using the OPLS model.

Nowadays, the calculation of the solid–solid equilibria and solid–fluid equilibria is almost routine. The usual methodology consists of several steps. First, the free energies corresponding to the different solid structures and the fluid phase at a certain thermodynamic state must be evaluated. To this end, it is common for the solid phases to use the Einstein crystal method⁴⁴ or the so-called Einstein molecule method,^{45,46} whereas the calculation of the fluid phase is usually performed through thermodynamic integration⁴⁷ from a state where the fluid behaves as an ideal gas. Once the free energies are computed at one thermodynamic state, these can be obtained at other states by again using thermodynamic integration.⁴⁷ Thus, the coexistence points are deduced in a simple way by comparing the chemical potentials of the different phases. Finally, the Gibbs–Duhem integration method^{48–50} allows one to draw the coexistence lines and thus the phase diagram. It should be commented that the first step can be also carried out by using a simple Hamiltonian integration⁴⁷ but only when the free energies of a model are known at a certain thermodynamic state. This methodology has been extensively used to evaluate the SSE and SFE of substances of different degrees of complexity, from simple models to molecular models [see review of Vega et al.⁴⁵ and references therein].

Besides this, the SSE and SFE can be quite useful for testing and improving the current intermolecular potentials. This conclusion was reached after a systematic study developed using the most popular models of water.^{45,51–57} Three-site models gave significantly poorer predictions of the phase diagram than those corresponding to the four-site models. Particularly, the TIP4P model provided the best predictions, although the melting points were far from the experimental values. Consequently, a reparametrization of this model, namely, TIP4P/2005, was suggested to obtain a better description of the phase diagram and the melting point. The performance of the TIP4P/2005 model was compared to a wide set of potentials with respect to ten properties, and it was shown to provide the best description of water capturing a great number of its anomalies. We believe that this approach can be used for evaluating and improving the intermolecular potential of other molecules such as methanol. Thus, the main goal of this work is to test the most popular models of methanol by calculating the solid–solid and solid–fluid equilibria and to assess the need of an improved potential. The set of properties to be tested was the coexistence lines in the p – T plane, the melting point, densities of the solid phases, and volume and enthalpy changes at melting. In addition, some results in the

Table 1. Lennard-Jones Parameters ϵ_a and σ_a , Partial Charges q_a , Geometries, and Dipole Moments μ_D of the Potential Models Used

site a	ϵ_a/k (K)	σ_a (Å)	q_a (e)	geometry
H1 methanol, ^{21,22} $\mu_D = 2.33$ D				
O	87.94	3.083	−0.728	O–H: 0.9451 Å
H	0.0	0.0	0.421	C–O: 1.4246 Å
C	91.15	3.861	0.297	C–O–H: 108.53°
OPLS methanol, ²⁰ $\mu_D = 2.22$ D				
O	85.546821	3.070	−0.700	O–H: 0.945 Å
H	0.0	0.0	0.435	C–O: 1.430 Å
C	104.16583	3.775	0.265	C–O–H: 108.5°
L2 methanol, ^{27,28} $\mu_D = 2.14$ D				
O	87.879	3.03	−0.67874	O–H: 0.9451 Å
H	0.0	0.0	0.43128	C–O: 1.4246 Å
C	120.5920	3.7543	0.24746	C–O–H: 108.53°
L1 methanol, ²³ $\mu_D = 2.22$ D				
O	86.5	3.03	−0.700	O–H: 0.9451 Å
H	0.0	0.0	0.435	C–O: 1.4246 Å
C	105.2	3.740	0.265	C–O–H: 108.53°

fluid phase such as the densities and vaporization enthalpy at room conditions and the critical temperature were included for completeness. Calculations of the SSE and the SFE were only made for the H1, L2, and L1 models since the corresponding ones for the OPLS model were recently published by the authors. Another aim is to provide the melting points for those researchers that use these models to describe methanol, a quantity especially useful for studying supercooled methanol.

MODELS, METHODOLOGY, AND SIMULATION DETAILS

As has been stated, the four models H1, OPLS, L2, and L1 have the same site definition and molecular geometry. They consist of three sites located on the methyl group (C), the oxygen atom (O), and the hydrogen (H) of the hydroxyl. Two Lennard-Jones (LJ) centers are located in the C and O sites (no Lennard-Jones center is placed on the H site as occurs in water), whereas charges are located on the three sites. The molecular geometry (bond distances and angles) and the dipole moments μ_D are given in Table 1, as well as the values corresponding to the Lennard-Jones (LJ) parameters, ϵ and σ , and the charges q of the sites. For these models, the intermolecular interactions between sites, a and b, are described by the site–site potential defined as follows

$$U_{ab} = 4 \cdot \epsilon_{ab} \cdot \left(\left(\frac{\sigma_{ab}}{r_{ab}} \right)^{12} - \left(\frac{\sigma_{ab}}{r_{ab}} \right)^6 \right) + \frac{q_a \cdot q_b}{r_{ab}} \quad (1)$$

where r_{ab} is the site–site distance. The LJ cross parameters σ_{ab} and ϵ_{ab} are computed from σ_a , σ_b and ϵ_a , ϵ_b , respectively, by using the Lorentz combining rules for the OPLS model and the Lorentz–Berthelot ones for the rest of the models. The potential energy between i and j molecules, U_{ij} , and that for a system of N molecules, U , are defined in the

following way

$$U_{ij} = \sum_a \sum_b U_{ab} \quad (2)$$

$$U = \sum_{i=1}^N \sum_{j>i}^N U_{ij} \quad (3)$$

The average potential energy per mole will be denoted with lowercase u .

In this work, three types of Monte Carlo simulations were performed: anisotropic NpT for solid phases of methanol, isotropic NpT for the fluid phase, and NVT simulations. The use of the anisotropic version of the NpT ensemble is absolutely required to simulate solid phases. It guarantees that the shape of the simulation box—and so the shape of the unit cell of the solid—is the equilibrium one and also that the solid is under hydrostatic pressure and free of stress (the pressure tensor will then be diagonal with the three components, being identical to the thermodynamic pressure). The number of molecules N corresponding to the solid phases α , β , and γ was 300, 320, and 270, respectively, as in our previous work⁴³ on the OPLS model. The number of molecules for each solid phase was chosen to fit at least twice the cutoff distance in each direction. This corresponds to $5 \times 5 \times 3$ unit cells for the α phase, $4 \times 4 \times 5$ for the β phase, and $3 \times 5 \times 3$ for the γ phase. The initial configuration used in the simulations was obtained from the experimental data of these structures after adjusting slightly the bond lengths and angles to the values of the H1, L2, and L1 models. Simulations of the fluid phase were performed with 300 molecules. In all the cases, equilibration lasted 20 000 cycles, and an additional 40 000 were generated for sampling (we define a cycle as a trial move per particle plus an attempt to change the volume of the system). The potential energy of our simulations was computed truncating the LJ site–site interactions at 10 Å except for the γ phase where 9 Å was set (due to the smaller size of the simulation box). Usual LJ long-range corrections⁵⁸ were applied. For the long-range Coulombic interactions, Ewald summation⁴⁷ was used. For the real space contribution of the Ewald sums, the same cutoff radius as for the LJ interactions was applied. The screening parameter and the number of the reciprocal space vectors were determined to achieve convergence in the real and the reciprocal space sum.

In our previous work⁴³ on the OPLS model, the Helmholtz (A) and the Gibbs (G) free energies were obtained by using the Einstein molecule method for the three solid phases and by thermodynamic integration from a state where methanol behaves as an ideal gas for the fluid phase. These calculations were performed at $T = 100$ K and $p = 1$ bar for α and β solid phases and at $T = 100$ K and $p = 4 \times 10^4$ bar for the γ phase. The reference state in which the free energy of the fluid phase was determined corresponds to $T = 298$ K and $p = 1$ bar conditions. Once the free energies of a reference model are known, the free energies of a new model can be easily obtained by using Hamiltonian integration⁴⁷ according to the expression

$$G(\lambda = 1) = G(\lambda = 0) + \int_0^1 \left(\frac{\partial G(\lambda)}{\partial \lambda} \right) d\lambda \quad (4)$$

In this equation, $G(\lambda)$ is the Gibbs free energy for a system with potential energy given by

$$U(\lambda) = (1 - \lambda)U_{\text{ref}} + \lambda U_{\text{new}} \quad (5)$$

where U_{ref} is the potential energy calculated by the intermolecular potential of a reference model (OPLS model in our case) and U_{new} is the same magnitude but for the new intermolecular potential which is being studied (H1, L2, or L1 in our case). Therefore, $G(\lambda = 0)$ is the Gibbs free energy of the reference model, and $G(\lambda = 1)$ is the Gibbs free energy of the new model, which were denoted as G_{ref} and G_{new} , respectively. The integrand of eq 4 takes the following form

$$\left(\frac{\partial G(\lambda)}{\partial \lambda} \right) = \langle (U_{\text{new}} - U_{\text{ref}}) \rangle_{\lambda} \quad (6)$$

i.e., it is evaluated as the average in the NpT ensemble of $(U_{\text{new}} - U_{\text{ref}})$ in a system with a Hamiltonian defined by eq 5 (subscript λ describes this point).

Therefore, for a specific new potential, we performed NpT simulations (anisotropic for the solids and isotropic for the fluid phase) to evaluate the average of eq 6 using the model described by eq 5. Ten different values of λ were considered. The results obtained from the averages were fitted to a fourth-degree polynomial in λ to perform the integration of eq 4 analytically. In this way, the Gibbs free energy of the new model was estimated. Notice that once the Gibbs free energy G is known the Helmholtz free energy A can be easily obtained by using the expression $G - pV = A$, and the chemical potential is simply evaluated as $\mu = G/N$.

As a cross-check of the methodology, the Gibbs free energy of the fluid phase was also computed using thermodynamic integration from a state where methanol behaves as an ideal gas. This calculation requires the simulation of the equation of state (EOS) along the isotherm $T = 800$ K from 1 bar to 0.1×10^4 bar and through an isochore from 800 to 298 K. The density corresponding to the isochore was $0.725 \text{ g} \cdot \text{cm}^{-3}$ for the H1 model, $0.788 \text{ g} \cdot \text{cm}^{-3}$ for the L2 model, and $0.786 \text{ g} \cdot \text{cm}^{-3}$ for the L1 model. All the details of the computation of the free energy from these simulations can be found elsewhere.⁴³

Once the free energy is known at a specific thermodynamic state, its value at other thermodynamic states can be easily determined by using thermodynamic integration. In that way, free energies were evaluated along the 1 bar isobar and the 100 K isotherm. In the first case, the following thermodynamic relation was used

$$\frac{G(T_2, p)}{NkT_2} = \frac{G(T_1, p)}{NkT_1} - \int_{T_1}^{T_2} \frac{H(T)}{NkT^2} dT \quad (7)$$

which allows one to obtain G at temperature T_2 and pressure p once G is known at temperature T_1 and pressure p . The integrand, where H denotes the enthalpy, is evaluated along the p isobar at selected temperatures between T_1 and T_2 by using NpT Monte Carlo simulations. In the second case, the following expression was applied

$$\frac{A(\rho_2, T)}{NkT} = \frac{A(\rho_1, T)}{NkT} + \int_{\rho_1}^{\rho_2} \frac{p(\rho)}{kT\rho^2} d\rho \quad (8)$$

where A at density ρ_2 and temperature T is calculated from the A value at density ρ_1 and temperature T . The integrand is evaluated along the T isotherm at specific pressures ranging from the density value ρ_1 to ρ_2 by using NpT simulations.

As has been stated previously, the chemical potential is calculated from the free energy G . Coexistence between two phases is obtained according to the condition of identical

chemical potential at a certain pressure and temperature. Once one coexistence point between two phases is determined, the rest of the coexistence curve was obtained by performing Gibbs–Duhem integration.^{48–50} This method, proposed by Kofke in 1993, is a numerical integration of the Clapeyron equation, which can be written as follows when two phases, labeled as I and II, coexist

$$\frac{dp}{dT} = \frac{h_{II} - h_I}{T(v_{II} - v_I)} \quad (9)$$

where lowercase denotes thermodynamic properties per mole. The differential equation can be integrated numerically since the enthalpy and volume differences between two phases can be easily calculated at a certain T and p . When implementing the Gibbs–Duhem integration, one obtains the coexistence pressure for the selected temperatures, the temperature acting as the independent variable. This is quite convenient when the coexistence line does not show a large slope in the p – T plane. However, when the slope is large the integration of the equation $dT/dp = T\Delta v_{I-II}/\Delta h_{I-II}$ is more efficient. A fourth-order Runge–Kutta algorithm was used to integrate the Clapeyron equation.

The vaporization enthalpy Δh_{l-v} was also calculated to permit a more complete comparison between the four models. This magnitude was obtained at $T = 298$ K as $\Delta h_{v-1} = -u_l + RT$ for the H1 model, where R denotes the universal gas constant and u_l is the average potential energy per mole of the liquid; for the rest of the models (L2, L1, and OPLS), it was computed at 298.15 K as $\Delta h_{v-1} = h_v - h_l$ by using the coexistence pressures given in refs 28 and 59. There is a growing acceptance of the idea that the self-energy correction⁶⁰ proposed by Berendsen for water could also be included in the calculation of Δh_{v-1} for other polar molecules with significant different dipole moment in the liquid and in the gas phase. This correction depends on that difference and can be approximated by

$$\Delta E_{\text{pol}} = (\mu_{D,1} - \mu_{D,g})^2 / 2\alpha \quad (10)$$

where α is the polarizability of methanol. Regarding the values of these magnitudes, the ones corresponding to $\mu_{D,1}$ for the different models are given in Table 1, $\mu_{D,g} = 1.7$ D, and $\alpha = 3.29$ Å³. This correction was evaluated and also included for the analysis.

RESULTS AND DISCUSSION

All the simulation data corresponding to the three models are provided in the Supporting Information of this work.

The values of the Helmholtz free energy A of α , β , γ , and fluid phases at several thermodynamic states (including the reference ones) are given in Table 2 for the different models. A comparison of the relative stability of the different solid phases can be performed at $T = 100$ K and $p = 1$ bar since at this pressure A/NkT is approximately equal to μ/kT . The γ phase takes, for all the

Table 2. Free Energies A , Densities ρ , and Average Potential Energies Per Mole u of the α , β , and γ Solid Phases and of the Fluid Phase of Methanol Obtained by the H1, OPLS, L2, and L1 Models at Temperature T and Pressure p

phase	p/bar	T/K	H1	OPLS	L2	L1
A/NkT						
α	1	100	−47.56	−49.09	−50.90	−51.27
β	1	100	−47.31	−48.93	−50.79	−51.09
γ^a	1	100	−43.93	−45.86	−47.39	−47.67
γ	4×10^4	100	−32.60	−35.22	−37.12	−37.42
fluid	1	298	−11.79		−12.60	−12.69
fluid ^b	1	298	−11.79	−12.18	−12.61	−12.69
$\rho/\text{g}\cdot\text{cm}^{-3}$						
α	1	100	0.984	1.024	1.034	1.052
β	1	100	0.986	1.024	1.034	1.051
γ	1	100	0.987	1.032	1.044	1.060
γ	4×10^4	100	1.262	1.305	1.305	1.333
fluid	1	298	0.725	0.760	0.788	0.786
$u/\text{kJ}\cdot\text{mol}^{-1}$						
α	1	100	−47.95	−49.30	−50.92	−51.27
β	1	100	−47.79	−49.18	−50.83	−51.13
γ	1	100	−45.06	−46.84	−48.18	−48.43
γ	4×10^4	100	−37.74	−39.84	−41.58	−41.88
fluid	1	298	−34.27	−35.67	−37.38	−37.86

^a Free energies evaluated using thermodynamic integration from the value at 4×10^4 bar. ^b Free energies evaluated using thermodynamic integration from the ideal gas state.

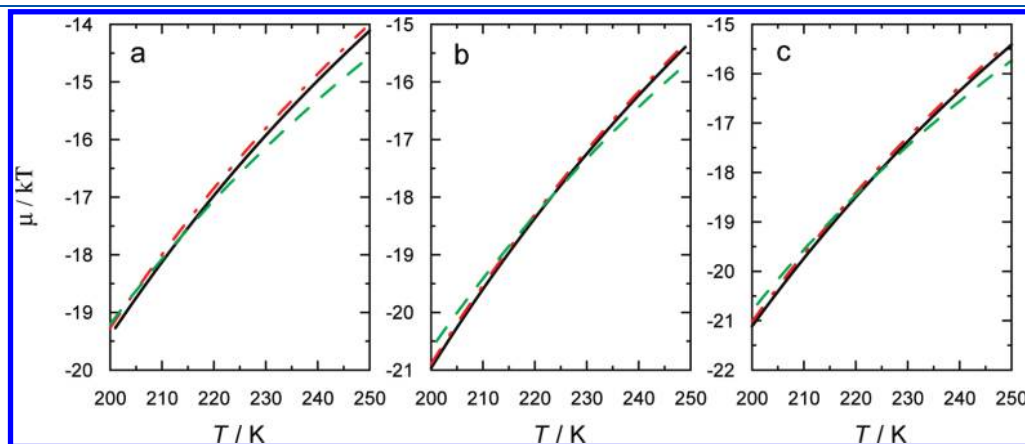


Figure 1. Chemical potential μ as a function of temperature T at 1 bar for fluid phase (green dashed) and for α (black solid) and β (red dashed-dotted) solid phases of methanol. (a) H1 model, (b) L2 model, and (c) L1 model.

models, significantly higher values than those of the β and α phases, which are very similar. This result indicates that the γ phase is considerably less stable at this state than the other phases, which is in agreement with the fact that this phase is only thermodynamically stable at high pressures in real methanol. Although the differences between the β and α phases are quite small, the α phase always takes lower A values, which means that it is the most stable phase at this thermodynamic state. On the other hand, to check our data obtained from eq 4, the free energy of the fluid was also calculated by using thermodynamic integration from the ideal gas as was done in ref 43. These last values, which are also shown in Table 2, differ by less than $0.01NkT$ from the results obtained by using Hamiltonian integration, providing further reliability in the accuracy of our calculations. The densities ρ and the average potential energies per mole u at these specific thermodynamic states are also given in Table 2. Notice that slight differences between α and β are appreciated for these magnitudes too.

As it was explained in Section II, the chemical potential μ of the α , β , γ , and fluid phases was computed as a function of temperature T (for $p = 1$ bar) and as a function of pressure (for $T = 100$ K). In Figure 1a, the chemical potentials μ corresponding to α , β , and fluid phases obtained by the H1 model are plotted against T at 1 bar (the γ phase is excluded since its chemical potential is significantly higher, as was shown before). As can be observed, the β phase takes higher values than the α phase over the whole temperature range studied. This fact indicates that the α phase is the most stable solid phase at that specific pressure. Regarding the fluid phase, its chemical potential takes higher values than the α phase below 214 K and lower ones from that temperature, so the coexistence temperature between α and fluid phase was 214 K. As for the β and fluid phase, the coexistence temperature was found at 204 K. Taking into account that the α phase is thermodynamically stable at this pressure, 214 K is the melting point of this model. The results corresponding to L2 and L1 models are shown in Figures 1b and 1c. As can be seen, the β phase is also metastable in these models, and coexistence temperatures of the α and β phases with the fluid phase were 223.5 K (the melting point) and 218.5 K, respectively, for the L2 model, and 223 K (the melting point) and 218 K for the L1 model. In summary, the β phase was found metastable at $p = 1$ bar for these models, as was found previously when using the OPLS model. In addition, the melting points predicted by all the models (215 K by OPLS) are far from 175.6 K, the experimental value (note that the melting point refers to the α -fluid

coexistence in the models, whereas this melting point refers to the β -fluid coexistence in the real methanol). The melting temperatures are summarized in Table 3. As for the stability of different solid phases along the 100 K isotherm (see Figure 2a, 2b, and 2c), the β phase was also found to be metastable for the H1, L2, and L1 models (as was found for OPLS). With regard to the H1 model, the α phase was the most stable below 15.6×10^4 bar, whereas for higher pressures γ is the stable phase. The coexistence pressure corresponding to the L2 model was 12.36×10^4 bar and 12.47×10^4 bar in the case of the L1 model (the value obtained by OPLS was of 11.50×10^4 bar). These results indicate that for the four models of this work the γ phase is stable for pressures much higher than found experimentally (3.5×10^4 bar).

The complete phase diagram of the four models considered in this work is plotted and compared to the experimental diagram in Figure 3. The experimental phase diagram¹⁹ is known only for pressures up to 1.5×10^4 bar. Experimentally only two coexistence curves have been reported: the first corresponds to the transition from the α to the β solid phase and for slightly higher temperatures the coexistence line between the β solid and the fluid. The single point presented in Figure 3 represents the only experimental thermodynamic state for which the existence of the γ phase has been reported. As can be seen, all the models are able to predict the existence of α , γ , and fluid phases, but the β phase is metastable in all the cases. However, this can not be considered as a dramatic failure of the models for two reasons. First, experimentally the region of stability of the experimental β -phase is very narrow, so the quantitative error is, thus, small. The second reason is that there is a strong similarity in both thermodynamics and structural properties for the α and β phases and so their competition in stability arises from the slight differences in the

Table 3. Melting Temperatures T_m for the H1, OPLS, L2, and L1 Models of Methanol^a

model	T_m /K
H1 ^{21,22}	214
OPLS ²⁰	215
L2 ^{27,28}	223.5
L1 ²³	223

^aThe experimental value of the melting temperature of methanol is 175.6 K.

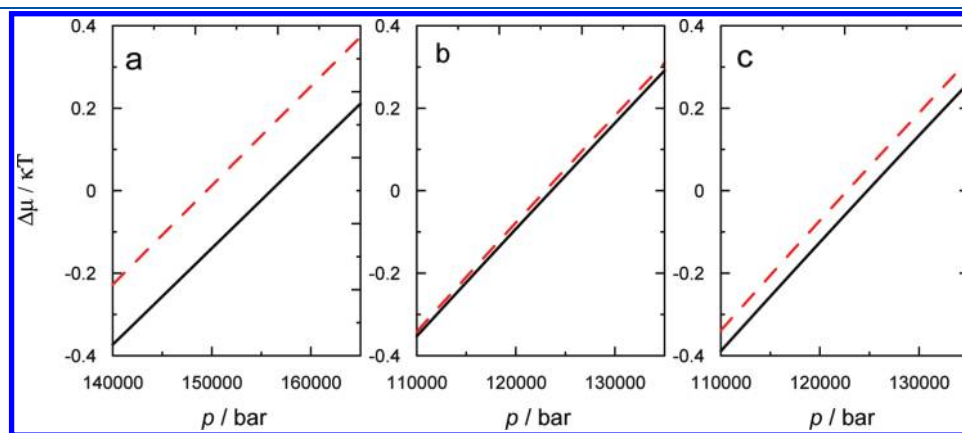


Figure 2. Difference between the chemical potential of α or β solid phases and that of γ solid phase of methanol plotted against pressure p at 100 K. α - γ (solid line) and β - γ (dashed line). (a) H1 model, (b) L2 model, and (c) L1 model.

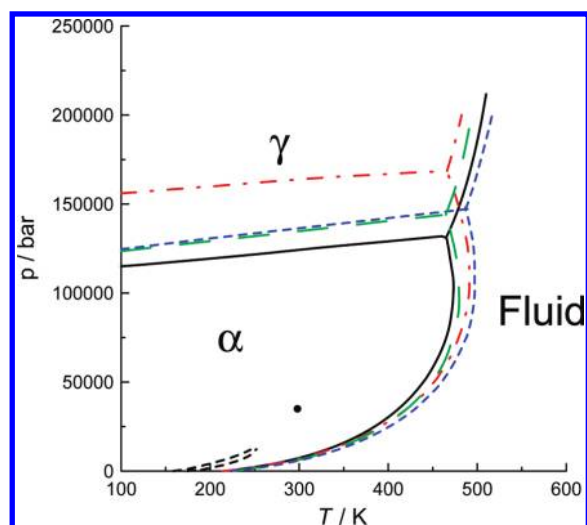


Figure 3. Phase diagram of H1 (red dashed-dotted), OPLS (black solid), L2 (green long-dashed), and L1 (blue short-dashed) methanol compared to the experimental one (black short-dashed). The experimental phase diagram was determined at pressures ranging between 1 and 1.5×10^4 bar, detecting two coexistence curves: going from low to high temperature, the first coexistence line represents the transition between the α solid phase and the β phase, and the second one defines the transition from the β phase to the fluid one. The single point symbolizes the only experimental thermodynamic state for which the existence of the γ phase was reported.

chemical potential along the p - T plane, which can only be captured using very accurate intermolecular potentials.

The coexistence lines presented in Figure 3 for the different models adopt a very similar shape. The α -fluid lines obtained by the four models are very close, and just some differences appear at high temperatures and pressures. A re-entrant melting curve is predicted in all the cases, and the melting points are almost the same, and far from the experimental. Regarding the α - γ line, the results obtained by the L2 and L1 models are very similar, whereas those corresponding to the H1 and OPLS models are located at higher and lower pressures, respectively. In any case, the stability of the γ phase is predicted in the models at very high pressures.

The properties at coexistence for the fluid- α and fluid- β transitions (at $p = 1$ bar) are presented in Table 4 and compared to the experimental results. In real methanol the fluid phase coexists with the β solid phase, but there is no coexistence between the α and fluid phase. Consequently, there are only experimental data corresponding to both enthalpy and volume transitions between the β and the fluid phase, whose values were taken from Riddick et al.⁶¹ and Staveley et al.¹⁴ However, an estimate of the “experimental” transition properties between the α -phase and the fluid was performed as the sum of the experimental β -fluid transition properties plus the experimental α - β transition one to make a comparison with the simulation results too. To this end, experimental volume and enthalpy α - β transition values were taken from Staveley et al.:¹⁴ $0.45 \text{ cm}^3 \cdot \text{mol}^{-1}$ and $0.636 \text{ kJ} \cdot \text{mol}^{-1}$, respectively. A great discrepancy between the model predictions and the experimental data can be appreciated. In addition, it must be noted that the three models provide similar estimates of the volume and enthalpy change at the transition.

The density ρ of the α , β , γ , and fluid phases at selected thermodynamic states (the residual internal energy is presented

Table 4. Coexistence Properties between the α or β Solid Phases and the Fluid Phase of Methanol for the H1, OPLS, L2, and L1 Models at 1 bar^a

model	H1	OPLS	L2	L1	exp.
α -fluid coexistence					
T_{coex}/K	214	215	223.5	223	175.6
$\rho_f/\text{g} \cdot \text{cm}^{-3}$	0.808	0.844	0.861	0.867	
$\rho_\alpha/\text{g} \cdot \text{cm}^{-3}$	0.926	0.964	0.972	0.988	
$\Delta v_{f,\alpha}/\text{cm}^3 \cdot \text{mol}^{-1}$	5.05	4.75	4.24	4.50	3.2 ^b
$h_f/\text{kJ} \cdot \text{mol}^{-1}$	-39.18	-40.51	-41.75	-42.42	
$h_\alpha/\text{kJ} \cdot \text{mol}^{-1}$	-44.37	-45.71	-47.06	-47.44	
$\Delta h_{f,\alpha}/\text{kJ} \cdot \text{mol}^{-1}$	5.19	5.20	5.31	5.02	3.85 ^b
β -fluid coexistence					
T_{coex}/K	204	209	218.5	218	
$\rho_f/\text{g} \cdot \text{cm}^{-3}$	0.820	0.847	0.862	0.871	
$\rho_\beta/\text{g} \cdot \text{cm}^{-3}$	0.934	0.971	0.978	0.998	
$\Delta v_{f,\beta}/\text{cm}^3 \cdot \text{mol}^{-1}$	4.76	4.80	4.43	4.57	2.75
$h_f/\text{kJ} \cdot \text{mol}^{-1}$	-39.70	-40.73	-42.29	-42.84	
$h_\beta/\text{kJ} \cdot \text{mol}^{-1}$	-44.52	-45.84	-47.17	-47.58	
$\Delta h_{f,\beta}/\text{kJ} \cdot \text{mol}^{-1}$	4.83	5.11	4.88	4.74	3.215

^a T_{coex} is the coexistence temperature; ρ_f , ρ_α , and ρ_β are the densities corresponding to the fluid and to the α and β solids; h_f , h_α , and h_β are the enthalpies (the term $3RT$ which arises from the translational and rotational kinetics terms is not included); $\Delta v_{f,\alpha}$, $\Delta v_{f,\beta}$ and $\Delta h_{f,\alpha}$, $\Delta h_{f,\beta}$ are the transition of both volumes and enthalpies for the fluid- α and the fluid- β coexistence at 1 bar. ^b Approximated value as explained in the text.

for completeness) and the vaporization enthalpy Δh_{v-1} (with and without the Berendsen correction) at 298.15 K obtained from the H1, OPLS, L2, and L1 models were compared with selected experimental data in Table 5. The experimental densities corresponding to the α and β phases were obtained from Torrie et al.,¹⁷ whereas those for the γ phase were taken from Allan et al.¹⁸ The model that shows the worst agreement with the experimental densities is the H1 one, which always gives too low values. Regarding α and fluid phases, both the L2 and L1 models provide the best predictions, whereas β and γ solid phases are better reproduced by the OPLS and L1 models, respectively. The experimental vaporization enthalpy was taken from Riddick et al.⁶¹ As for the simulation results obtained without the Berendsen term, it can be seen that the OPLS model shows the best agreement. When the Berendsen correction is applied (the values are given in parentheses in Table 5), it can be appreciated that the best agreement does not correspond to the OPLS model but to the L1 model, although results from the L2 model are also quite close to the experimental data. It was previously found⁵⁷ for water that models which reproduce the experimental critical temperature were able to predict the vaporization enthalpy only if the Berendsen correction is included. In our case, the critical temperatures of methanol determined by using the H1, OPLS, L2, and L1 models are 484, 500, 506, and 513 K,²³ respectively, and the experimental one is 513 K.⁶¹ Therefore, the same fact described for water is verified for methanol since the models which give the best critical temperature also provide the best vaporization enthalpy when the Berendsen term is applied. Notice however that differences between the experimental values and those of the models of methanol are small. Simulation data of the vaporization enthalpy

Table 5. Densities ρ and Average Potential Energies Per Mole u of the α , β , and γ Solid Phases and of the Fluid Phase of Methanol Obtained by the H1, OPLS, L2, and L1 Models at the Temperature T and Pressure p Compared to Experimental Data^a

phase	p/bar	T/K	H1	OPLS	L2	L1	exp.
			$\rho/\text{g}\cdot\text{cm}^{-3}$				
α	1	160	0.955	0.994	1.006	1.022	1.0147
β	1	170	0.953	0.991	1.003	1.019	0.9921
γ	4×10^4	298	1.235	1.276	1.277	1.304	1.3526
fluid	1	298	0.725	0.760	0.788	0.786	0.7864

phase	p/bar	T/K	H1	OPLS	L2	L1	exp.
			$u/\text{kJ}\cdot\text{mol}^{-1}$				
α	1	160	-46.17	-47.51	-49.14	-49.49	
β	1	170	-45.67	-47.11	-48.75	-49.06	
γ	4×10^4	298	-34.33		-38.17	-38.50	
fluid	1	298	-34.27	-35.67	-37.38	-37.86	

$\Delta h_{v-1}/\text{kJ}\cdot\text{mol}^{-1}$							
			36.75	37.66	38.90	39.67	
				37.40 ^b	39.14 ^c	39.90 ^b	37.43
			(34.46)	(35.56)	(36.79)	(37.50)	

^aVaporization enthalpy at room temperature Δh_{v-1} for the different methanol models, its value after including the Berendsen polarization correction (in parentheses), and the experimental one are also shown. ^bFrom ref 59. ^cFrom ref 27.

of previous works^{27,59} were also included to show the close agreement with our numbers.

In this point, a global analysis of the performance of the models seems to be appropriate. The four models predict correctly the higher stability of the α phase with respect to the γ phase at low pressures, the overall shape of the fluid- α coexistence line, and the similarity in thermodynamic properties of the α and β phases. The β phase was found slightly less stable than the α phase, but as it was previously commented this fact must not be considered as a strong failure. Thus, the description is qualitatively correct. However, there are important quantitative discrepancies. For instance, the pressure of the α - γ coexistence line is too high, and the same is true for the melting point temperature at room pressure. The description of the transition properties at melting (i.e., volume change, enthalpy change) is not very good either. Concerning the fluid phase, the L1 model gives the best predictions, and the L2 model shows also good agreement with experiment. This is not strange since these models were parametrized forcing their parameters to reproduce the vapor-liquid equilibrium and properties of the fluid at room conditions. As for the densities of the solid phases, the L1 model provides the best predictions from a global point of view although the β phase is best reproduced by the OPLS model. Thus, putting all the information together, it can be concluded that the best model of methanol is the L1 model due mainly to its reliability in the fluid phase. However, the discrepancies exposed above related with the SSE and SFE indicate that there is room for improvement; a new parametrization based on the phase diagram calculations could improve the quality of the results. All these considerations can be appreciated quantitatively in Table 6 where the percent relative deviation PRD between the simulation data for each model of methanol and the experimental value is

Table 6. Percent Relative Deviations PRD Obtained from the Simulation Data for Each Model of Methanol and the Experimental Value for a Set of Thermodynamic Properties^a

property	PRD/%			
	H1	OPLS	L2	L1
Δh_{v-1} ^b	7.9	5.0	1.7	0.2
T_c	5.7	2.5	1.4	0.0
ρ_f	7.8	3.4	0.2	0.1
ρ_α	5.9	2.0	0.9	0.7
ρ_β	3.9	0.1	1.1	2.7
ρ_γ	8.7	5.7	5.6	3.6
T_m	22	22	27	27
$p_{\text{coex},\alpha-\gamma}$	346	229	253	256
$\Delta h_{f,\beta}$	50	59	52	47
$\Delta v_{f,\beta}$	73	75	61	66

^a Δh_{v-1} is the vaporization enthalpy at 298.15 K. T_c is the critical temperature. ρ_α , ρ_β , ρ_γ , and ρ_f denote the densities of the α , β , γ , and fluid phases at the thermodynamic state given in Table 5. T_m is the melting temperature. $p_{\text{coex},\alpha-\gamma}$ is the coexistence pressure between the α and γ phases at 100 K. $\Delta h_{f,\beta}$ and $\Delta v_{f,\beta}$ are the transition enthalpy and volume for the coexistence between the β phase and the fluid at 1 bar. ^bComputed with the Berendsen correction.

presented in Table 6 for all these thermodynamic properties. The PRD parameter was computed as follows

$$\text{PRD} = \left| \frac{y^{\text{sim}} - y^{\text{exp}}}{y^{\text{exp}}} \right| \cdot 100 \quad (11)$$

where y is the thermodynamic property and the superscripts sim and exp denote simulation and experimental. Note that this table allows us also to establish particularly when and where each force field should be reliable. From the results presented in Table 6, it can be seen that L1 provides the best agreement with experiment for most of the properties, although the predictions of L2 are also quite good.

All evidence available so far indicates the possible origin of the failure of all the models in the prediction of the SSE and the SFE. On one hand, the vaporization enthalpies of all the models are very close since they deviate not much from the experimental. It seems to indicate that the strength of the hydrogen bond predicted by the models in the fluid phase is roughly correct. On the other hand, the great stability of the α phase (or β since its free energy is quite similar) in relation to the fluid phase translates into a high melting temperature and enthalpy which seems to indicate that the hydrogen bonds in the α solid are too strong. The high values of the α - γ transition pressures also suggests that the strength of the hydrogen bond in the α phase is too large. An improved potential should modify the charge distribution to decrease the strength of the hydrogen bond in the α phase. In fact, previous work on water has shown that slightly modifying the charge distribution in the molecule produces important changes in the phase diagram. The same probably applies to methanol, although of course the simplified description of the interaction between methanol molecules of the type used in this work does not allow us to describe all its properties. As a final remark, it should be pointed out that the majority of water models underestimates the melting temperature and the melting enthalpy, whereas the opposite seems to occur for methanol. This is so even though models describe the vaporization enthalpy reasonably well in both cases. This fact

suggests that models fitted to reproduce the vapor–liquid equilibrium can either overestimate (as found here for methanol) or underestimate the melting temperature, as happens for water.

CONCLUSIONS

The solid–solid and solid–fluid equilibria were considered to test the most popular models of methanol (H1, OPLS, L2, and L1). In this work, the free energies for the H1, L2, and L1 models were determined by using the Hamiltonian integration method considering the OPLS as the reference model since its phase diagram and free energies are known from previous work. Afterward, thermodynamic integration was used to estimate the initial coexistence points, and then the complete phase diagram was drawn from those initial points by using the Gibbs–Duhem integration procedure. Results can be summarized as follows. The four considered models were able to predict the thermodynamic stability of the α , γ , and fluid phases. The overall shape of the coexistence lines was almost the same for the four models. The β solid, a thermodynamically stable phase in real methanol, was found metastable for the four potential models. Likewise, they predict a similar location of the fluid– α line with the melting points belonging to a very narrow temperature interval, 214–223 K, and differing by about 40 K from the experimental value (175.6 K). The overestimation of the melting point is correlated to the overestimation of the melting enthalpy. Besides, the models overestimate the pressure of the α – γ line: the γ phase is stable at pressures above 11×10^4 bar for the OPLS and above 16×10^4 bar for the H1 model. This result is in contrast with the fact that the γ phase is just stable at 3.5×10^4 bar in real methanol. In summary, all the models provide an equivalent and qualitatively correct picture of the phase diagram of methanol. Taking into account that the L1 model provides the best predictions of the vaporization enthalpy, the critical temperature, and the density of the fluid at room conditions, we select L1 as the best model of methanol among those considered in this work, followed closely by L2 (which can also be applied successfully to water–methanol mixtures⁶²). However, it is clear that there is room for improvement. Some progress can still probably be obtained by modifying the parameters while still using simple rigid nonpolarizable models, most likely by modifying the geometry of the charge distribution. However, more dramatic improvements may require a more sophisticated description of the interaction between methanol molecules: inclusion of flexibility, polarization, three-body forces, and nuclear quantum effects may indeed be needed.

ASSOCIATED CONTENT

S Supporting Information. The free energies and densities obtained from Hamiltonian integration simulations are given in Tables A.1–A.3. The EOS of the different solid phases and the fluid phase determined for thermodynamic integration are shown in Tables A.4–A.8. Finally, the coexistence properties, including pressure and temperature of coexistence as well as the densities and enthalpies calculated in the Gibbs–Duhem integration, are summarized in Tables A.9–A.17. This material is available free of charge via the Internet at <http://pubs.acs.org>.

AUTHOR INFORMATION

Corresponding Author

*E-mail: dgs@uvigo.es.

ACKNOWLEDGMENT

The authors are grateful to the Dirección Xeral de I + D da Xunta de Galicia (projects PGIDIT-06-PXIB-3832828-PR and INCITE08E1R383012ES), Ministerio de Educación y Ciencia (project FIS2010-16159), and Universidad de Vigo (project 08VI-A12) for financial support, to the Social European Fund and the “Dirección Xeral de Ordenación e Calidade do Sistema Universitario de Galicia” from the “Consellería de Educación e Ordenación Universitaria-Xunta de Galicia” for grant funding to ADP, and to the “Ministerio de Educación y Ciencia” under the “Programa Nacional de Formación del Profesorado Universitario” (#AP-2007-02165 and #AP-2007-02172) for supporting the research of PGA and JMD. We thank Dr. Carl McBride for a critical reading of the manuscript, Dr. Jadran Vrabc for providing us simulation data for comparison, and the referees for their useful suggestions.

REFERENCES

- (1) Piermarini, G. J.; Block, S.; Barnett, J. D. *J. Appl. Phys.* **1973**, *44*, 5377–5382.
- (2) Brown, J. M.; Slutsky, L. J.; Nelson, K. A.; Cheng, L.-T. *Science* **1988**, *241*, 65–67.
- (3) Luo, M.; Song, Y.; Dai, L. L. *J. Chem. Phys.* **2009**, *131*, 194703.
- (4) Sloan, E. D. *Nature (London)* **2003**, *426*, 353–359.
- (5) Nichols, R. J. *J. Sci. Ind. Res.* **2003**, *62*, 97–105.
- (6) Duffie, J. A.; Beckman, W. A. *Solar Engineering of Thermal Processes*; Wiley: New York, 1992.
- (7) Ball, P. *Chem. Rev.* **2008**, *108*, 74–108.
- (8) de Reuck, K. M.; Craven, R. J. B. *Methanol. International Thermodynamic Tables of the Fluid State-12*; Blackwell: Oxford, 1993.
- (9) Aliev, M. M.; Magee, J. W.; Abdulagatov, I. M. *Int. J. Thermophys.* **2003**, *24* (6), 1527–1549.
- (10) TRC *Thermodynamics Tables, Non-Hydrocarbons*; Thermodynamics Research Center: TX, 1996.
- (11) Zabransky, M.; Ruzicka, V.; Domalsky, E. S. *Heat Capacities of Liquids, Critical Review and Recommended Values*; American Chemical Society: Washington, DC, 1996.
- (12) Parks, G. S. *J. Am. Chem. Soc.* **1925**, *47*, 338–345.
- (13) Kelley, K. K. *J. Am. Chem. Soc.* **1929**, *51*, 180–187.
- (14) Staveley, L. A. K.; Hogg, M. A. P. *J. Chem. Soc.* **1954**, *1954*, 1013–1016.
- (15) Torrie, B. H.; Weng, S.-X.; Powell, B. M. *Mol. Phys.* **1989**, *67* (3), 575–581.
- (16) Tauer, K. J.; Lipscomb, W. N. *Acta Crystallogr.* **1952**, *5*, 606–612.
- (17) Torrie, B. H.; Binbrek, O. S.; Strauss, M.; Swainson, I. P. *J. Solid State Chem.* **2002**, *166*, 415–420.
- (18) Allan, D. R.; Clark, S. J.; Brugmans, M. J. P.; Ackland, G. J.; Vos, W. L. *Phys. Rev. B* **1998**, *58*, R11809–812.
- (19) Gromnitskaya, E. L.; Stal’gorova, O. V.; Yagafarov, O. F.; Brazhkin, V. V.; Lyapin, A. G.; Popova, S. V. *JETP Lett.* **2004**, *80* (9), 597–601.
- (20) Jorgensen, W. L. *J. Phys. Chem.* **1986**, *90*, 1276–1284.
- (21) Haughney, M.; Ferrario, M.; McDonald, I. R. *Mol. Phys.* **1986**, *58*, 849–853.
- (22) Haughney, M.; Ferrario, M.; McDonald, I. R. *J. Phys. Chem.* **1987**, *91*, 4934–4940.
- (23) van Leeuwen, M. E.; Smit, B. *J. Phys. Chem.* **1995**, *99*, 1831–1833.
- (24) Jorgensen, W. L. *J. Am. Chem. Soc.* **1981**, *103*, 341–345.
- (25) Stouten, P. F. W.; Kroon, J. *J. Mol. Struct.* **1988**, *177*, 467–475.
- (26) Stouten, P. F. W.; van Eijck, B. P.; Kroon, J. *J. Mol. Struct.* **1991**, *243*, 61–87.
- (27) Schnabel, T.; Srivastava, A.; Vrabc, J.; Hasse, H. *J. Phys. Chem. B* **2007**, *111*, 9871–9878.

- (28) Guevara-Carrion, G.; Nieto-Draghi, C.; Vrabec, J.; Hasse, H. *J. Phys. Chem. B* **2008**, *112*, 16664–16674.
- (29) Weerasinghe, S.; Smith, P. E. *J. Phys. Chem. B* **2005**, *109*, 15080–15086.
- (30) Walsler, R.; Mark, A. E.; van Gunsteren, W. F.; Lauterbach, M.; Wipff, G. *J. Chem. Phys.* **2000**, *112* (23), 10450–10459.
- (31) Palinkas, G.; Hawlicka, E.; Heinzinger, K. *J. Phys. Chem.* **1987**, *91* (16), 4334–4341.
- (32) Jorgensen, W. L.; Maxwell, D. S.; Tirado-Rives, J. *J. Am. Chem. Soc.* **1996**, *118* (45), 11225–11236.
- (33) Cornell, W. D.; Cieplak, P.; Bayly, C. I.; Gould, I. R.; Merz, K. M.; Ferguson, D. M.; Spellmeyer, D. C.; Fox, T.; Caldwell, J. W.; Kollman, P. A. *J. Am. Chem. Soc.* **1995**, *117* (19), 5179–5197.
- (34) Chen, B.; Potoff, J. J.; Siepmann, J. I. *J. Phys. Chem. B* **2001**, *105* (15), 3093–3104.
- (35) Ferrando, N.; Lachet, V.; Teuler, J. M.; Boutin, A. *J. Phys. Chem. B* **2009**, *113*, 5985–5995.
- (36) Skaf, M. S.; Fonseca, T.; Ladanyi, B. M. *J. Chem. Phys.* **1993**, *98* (11), 8929–8945.
- (37) Yu, H.; Geerke, D. P.; Liu, H.; van Gunsteren, W. F. *J. Comput. Chem.* **2006**, *27* (13), 1494–1504.
- (38) Gao, J.; Habibollahzadeh, D.; Shao, L. *J. Phys. Chem.* **1995**, *99*, 16460–16467.
- (39) Caldwell, J. W.; Kollman, P. A. *J. Phys. Chem.* **1995**, *99*, 6208–6219.
- (40) Dang, L. X.; Chang, T.-M. *J. Chem. Phys.* **2003**, *119* (18), 9851–9857.
- (41) Patel, S.; Brooks, C. L., III. *J. Chem. Phys.* **2005**, *122*, 024508.
- (42) Harmony, M. D.; Laurie, V. W.; Kuczukowski, R. L.; Schwendeman, R. H.; Ramsay, D. A.; Lovas, F. J.; Lafferty, W. J.; Maki, A. G. *J. Phys. Chem. Ref. Data* **1979**, *8*, 619–721.
- (43) Salgado, D. G.; Vega, C. *J. Chem. Phys.* **2010**, *132*, 094505.
- (44) Frenkel, D.; Ladd, A. J. C. *J. Chem. Phys.* **1984**, *81*, 3188–3193.
- (45) Vega, C.; Sanz, E.; Abascal, J. L. F.; Noya, E. G. *J. Phys.: Condens. Matter* **2008**, *20*, 153101.
- (46) Noya, E. G.; Conde, M. M.; Vega, C. *J. Chem. Phys.* **2008**, *129*, 104704.
- (47) Frenkel, D.; Smit, B. *Understanding Molecular Simulation*; Academic Press: New York, 2002.
- (48) Kofke, D. A. *J. Chem. Phys.* **1993**, *98*, 4149–4162.
- (49) Kofke, D. A. *Mol. Phys.* **1993**, *78*, 1331–1336.
- (50) Kofke, D. A. In *Monte Carlo Methods in Chemical Physics*; Ferguson, D. M., Siepmann, J. I., Truhlar, D. G., Ed.; Wiley: New York, 1998.
- (51) Sanz, E.; Vega, C.; Abascal, J. L. F.; MacDowell, L. G. *Phys. Rev. Lett.* **2004**, *92*, 255701.
- (52) Sanz, E.; Vega, C.; Abascal, J. L. F.; MacDowell, L. G. *J. Chem. Phys.* **2004**, *121*, 1165–1166.
- (53) Vega, C.; Sanz, E.; Abascal, J. L. F. *J. Chem. Phys.* **2005**, *122*, 114507.
- (54) Abascal, J. L. F.; Sanz, E.; Garcia, R.; Vega, C. *J. Chem. Phys.* **2005**, *122*, 234511.
- (55) Vega, C.; Abascal, J. L. F. *J. Chem. Phys.* **2005**, *123*, 144504.
- (56) Abascal, J. L. F.; Vega, C. *J. Chem. Phys.* **2005**, *123*, 234505.
- (57) Vega, C.; Abascal, J. L. F.; Conde, M. M.; Aragonés, J. L. *Faraday Discuss.* **2009**, *141*, 251–276.
- (58) Allen, M. P.; Tildesley, D. J. *Computer Simulation of Liquids*; Oxford University Press: Oxford, 1987.
- (59) Lisal, M.; Smith, W. R.; Nezbeda, I. *Fluid Phase Equilib.* **2001**, *181*, 127–146.
- (60) Berendsen, H. J. C.; Grigera, J. R.; Straatsma, T. P. *J. Phys. Chem.* **1987**, *91*, 6269–6271.
- (61) Riddick, J.; Bunger, W. B.; Sakano, T. *Organic Solvents. Physical Properties and Methods of Purification*; Wiley: New York, 1986.
- (62) Guevara-Carrion, G.; Vrabec, J.; Hasse, H. *J. Chem. Phys.* **2011**, *134*, 074508.